Elasto-plastic response of reversibly crosslinked biopolymer bundles

Poulomi Sadhukhan, Ole Schuman and Claus Heussinger

Institute for Theoretical Physics, Georg-August University of Göttingen, Friedrich-Hund Platz 1, 37077 Göttingen, Germany

the date of receipt and acceptance should be inserted later

Abstract. We study the response of F-actin bundles to driving forces through a simple analytical model. We consider two filaments connected by reversibly bound crosslinks and driven by an external force. Two failure modes under load can be defined. *Brittle failure* is observed when crosslinks suddenly and collectively unbind, leading to catastrophic loss of bundle integrity. During *ductile failure*, on the other hand, bundle integrity is maintained, however at the cost of crosslink reorganization and defect formation. We present phase diagrams for the onset of failure, highlighting the importance of the crosslink stiffness for these processes. Crossing the phase boundaries, force-deflection curves display (frequency-dependent) hysteresis loops, reflecting the first-order character of the failure processes. We evidence how the introduction of defects can lead to complex elasto-plastic relaxation processes, once the force is switched off. Depending on, both, the time-scale for defect motion as well as the crosslink stiffness, bundles can remain in a quasi-permanent plastically deformed state for a very long time.

1 Introduction

Actin is one of the the most prominent examples of a protein that can polymerize into long filamentous polymers (f-actin). In combination with some of the many different actin-binding proteins ("crosslinks") these filaments can then assemble into a wealth of higher-order cytoskeletal structures, with a multitude of different biological functions. On a fundamental level it is an interplay between the energy scales of crosslink and filament deformations that determines the mechanical properties of these structures. The dynamical properties are governed, among other factors, by the reversibility of the filament-crosslink bond, which has an intrinsic and finite lifetime. In living cells, dynamic crosslinking is needed to facilitate the rearrangement of the cytoskeleton under external mechanical and chemical forces. This results into dissipation of memory of initial states and stabilization in new configurations under changing environment. Under load, reversible crosslinking can be one pathway for stress release. Consequences may be internal rearrangements, large-scale structure formation, creep or even catastrophic failure.

Apart from complex cytoskeletal networks, actin filaments are also found to assemble into simple structures with only few filaments. For example one can observe kinked helices, rings, tennis-racket shapes due to a competition between elastic and interfacial effects [1,2]. The

Correspondence to: sadhukhan@theorie.physik.uni-goettingen.de, heussinger@theorie.physik.uni-goettingen.de

coiled acrosome is composed of straight sections of bundled actin filaments joined via kinks [3]. A racket shape is also observed in a tubulin rod that had buckled inside of a vesicle [4].

Here, we consider the arguably simplest filament assembly: that of two filaments crosslinked together in a parallel fashion to form a bundle.

F-actin bundles are plenty in cytoskeletal structures in eukaryotes. They provide mechanical stability in filopodia, microvilli, stereocilia stress fibers and the sperm acrosome, play roles in various cellular functions like locomotion [5, 6,7], mechanotransduction [8] and fertilization. Some invitro experimental studies reveal that the crosslinking proteins and their interactions with the filaments have important effects on the mechanical and the structural properties of the bundle assemblies [9,10,11,12,13,14,15]. Under the assumption of permanently bound crosslinks, a theoretical description has been developed ("wormlike bundle" model) to characterize bundle mechanics [16,17]. Theoretical work has also focused on thermal denaturation [18, 19], thermally assisted force-induced desorption [20], or the effects of filament helicity on bundle structure and stability [21,22].

In recent experiments [23], the time dependent effects of large bundle deformation has been studied in-vitro. These experiments highlight the important aspect of "crosslink remodelling", which has not been accounted for in these previous studies: in response to force, crosslinks will repeatedly un- and rebind at different binding sites along

the actin filament. In the experiments, a crosslinked f-actin bundle is subjected to a stress and kept in a bent state for a short period (10s) or a long period (1000s). After this waiting time, the bundle was released and the relaxation was observed with time. For short waiting time, the bundle relaxes back exponentially to its initial straight ground state. It behaves elastically. For the long waiting times, however, the bundle only partially relaxes back and a substantial residual bending deformation remained in the bundle, which is therefore plastically deformed. It seems that upon deformation, new crosslink binding sites become available which allow to reduce the strain on the crosslinks and thus are more favourable. After release of the force, these new connections stabilize the bent conformation and thus the bundle remains in a bent form.

This transition from elastic to plastic response of the filament bundle is the subject of this paper. We will show how already a simple two-filament bundle can display complex mechanical properties. With the help of case-studies we can define two failure modes of the bundle under load. *Brittle failure* is observed when crosslinks unbind under load [24,25], leading to catastrophic loss of bundle integrity. *Ductile failure* maintains bundle integrity at the cost of crosslink remodelling and defect formation.

The paper is organized as follows. In Sect.2, we describe our model. Two different cases of crosslink binding are considered. The results are discussed in Sect.3. We show that bundle deformation leads to crosslink unbinding processes that crucially depend on the stiffness of the crosslinking protein. The Sect. 3.1 and Sect.3.2 discuss the two above mentioned scenarios. A time-dependent force is introduced in Sect.4. There we show how the response changes with the frequency of the driving force, and also consider the relaxation of the bundle once the force is switched off. Finally, in Sect.5, we summarize our results.

2 Model

We consider a biopolymer bundle of length L, lying in a two-dimensional plane and consisting of two parallel inextensible actin filaments. A schematic diagram of such a bundle is shown in Fig.1. In a variety of systems such as organic and inorganic nanotubes as well as stiff biopolymers, the stretching deformation mode is energetically expensive relative to the bending mode, so that the filaments may be approximated as inextensible. We comment on the effect of filament stretching at the end of Sect. 3. The filaments are laterally interconnected by reversible crosslinks (red lines in Fig.1) they can dynamically bind and unbind the filament pair.

On each filament there are $N_\times$ crosslink binding sites, spaced at regular intervals a distance δ apart. One end of the bundle is grafted at a wall and the other end is free to move. The force is applied at the free end which produces a bending deformation in the bundle creating stress on the crosslinks. The boundary conditions resemble the in vitro experiments done by D. Strehle et. al [23], where the free end is subjected to a force by pulling it while the other end is immobilized by sticking to a heavy bead. Because of
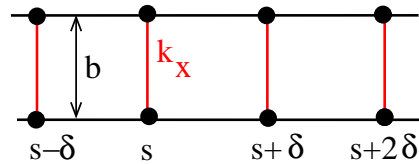

Fig. 1. Schematic diagram of an F-actin bundle with two filaments. Two black lines represent the filaments. The black circles show the crosslink binding sites on the filaments. The red vertical lines represent the crosslinks connecting two filaments. The distance between two crosslink binding sites is δ and the lateral distance between the filaments is b. The crosslink stiffness is denoted by $k_\times$.

the driving force, the bundle will be deformed by bending the filaments and shearing the crosslinks (see Fig.2). The shearing energy [26,27,28,29] of the crosslinks amounts to

$$H_{sh} = \frac{k_\times}{2\delta} \int_0^L (b\theta(s))^2 \, ds, \qquad (1)$$

where b is the separation between the two filaments and $k_\times$ is the crosslink stiffness, or the mechanical stiffness of the crosslinking agent. Here $\theta(s)$ is the angle of inclination, i.e. angle of the local tangent the bent bundle makes at a point s with respect to the initial configuration, s being the arc length along the bundle. The quantity $b\theta(s)$, therefore, gives the amount of shear in the crosslink at s. The bending energy of the filaments can be obtained from
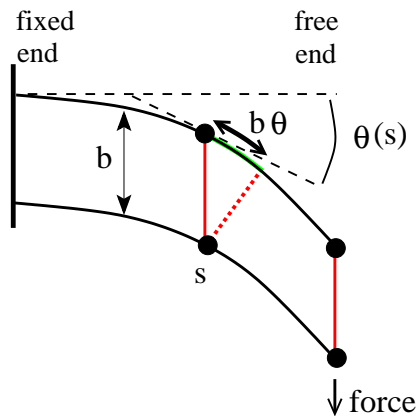

Fig. 2. A bent configuration of a crosslinked filament bundle. Bending by an angle θ leads to crosslink sliding and a shear deformation of amplitude $b\theta$.

WLC Hamiltonian as

$$H_b = \kappa_f \int_0^L \theta'^2(s) \, ds, \qquad (2)$$

where κ_f is the bending stiffness of the filaments. There is another contribution coming in the Hamiltonian due the driving force f at the free end, which reads,

$$H_f = -2f \int_0^L \theta(s) \, ds. \qquad (3)$$

In our calculations we use a linearized forcing term $\sim f\theta$, which is only accurate for small deflections. For typical experiments large deflections may be important, and the full expression $f\sin(\theta)$ would have to be used. We have checked in some cases that this would not change the qualitative behaviour of the bundle response under stress. Moreover, considering the small θ approximation keeps the model solvable analytically.

The total Hamiltonian of the system is then the sum of the three contributions, $H = H_{sh} + H_b + H_f$.

The most favourable configuration is chosen by the system by minimizing energy. In doing so, some crosslinks may unbind from the binding sites to cope with the force. This results in a change in the crosslink density in the bundle depending on the magnitude of the applied force, the stiffness of the crosslinks and bending stiffness of the bundle. To proceed with the analytical calculations, we introduce the crosslink density,

$$n = \text{number of bound crosslinks}/N_\times$$

in a mean field way which effectively normalizes the crosslink stiffness $k_\times \to nk_\times$ in Eq.(3) [25,24]. The crosslink density n can vary from 0 (all crosslinks unbound) to 1 (all crosslinks bound). There are two other contributions in the energy, one is from the entropy of mixing, $E_{mix} = k_BT[n\ln n + (1-n)\ln(1-n)]$ and the other is μn, where μ is the chemical potential for crosslink binding.

We modify the problem of unbinding of crosslinks in a way to allow the crosslinks to rebind to new crosslink binding sites. To simplify things, let us allow the crosslinks to rebind only to the right neighbouring site, i.e. allow connections between site α of 1st filament and sites α as well as $\alpha + 1$ on the 2nd filament (see Fig.3). The rebinding
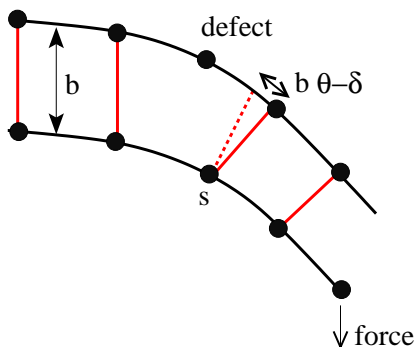

Fig. 3. A bent configuration of a forced crosslinked filament bundle. Rebinding of crosslinks has taken place to new binding sites after holding the bundle in bent configuration. The red dotted line shows the crosslink in undeformed state. The rebinding creates a defect in the bundle.

will result in a mismatch in the crosslink binding registry between the two filaments. The starting point of such mismatch will look like a "defect" with one vacant binding site in one filament (Fig.3b). We will only allow for one defect in the following. If s_D is the defect site, all the crosslinks

situated at $s > s_D$ will be rebound to the shifted registry. This can be incorporated into the Hamiltonian by modifying the shearing energy as,

$$H_{sh} = \frac{k_\times}{2\delta} \int_0^L (b\theta(s) - d(s))^2 \, ds, \qquad (4)$$

where $d(s)$ is the relative shift in the crosslinking sites in the two filaments. It goes from zero to δ when going through the defect. For convenience we choose the following continuously differentiable form

$$d(s) = \begin{cases} 0, & s \le s_D - \delta, \\ \frac{\delta}{2}\left(1 + \sin\frac{\pi(s-s_D)}{2\delta}\right), & s_D - \delta < s < s_D + \delta, \\ \delta, & s \ge s_D + \delta. \end{cases}$$
$$(5)$$

Here we assume that the defect has a core region of size 2δ, from $s_D - \delta$ to $s_D + \delta$. Note that here we set $n = 1$ as we do not allow any open crosslink.

The total Hamiltonian is minimized with respect to θ to find the corresponding differential equation. The solution for $\theta(s)$ is then plugged back into the Hamiltonian to find the energy. The numerical calculations have been done with the following parameters. The intercrosslink spacing δ and the separation between the filaments b are taken as $b = \delta = 1$. In actin filaments the crosslink sites can be taken to be roughly $40nm$ apart, which corresponds to the helical repeat of the filament [9]. The bending stiffness $\kappa_f = 1$, sets the energy scale in all the results. The length of the bundle and the persistence length are taken as $L = l_p = 500$, which correspond to $\sim 20\mu m$ [30]. Temperature is fixed via $(k_BT)^{-1} = l_p/\kappa_f = 500$. The most important parameter in this work is the ratio $k_\times/\kappa_f$. We refer to this ratio whenever we say $k_\times$ in this paper. Stiff crosslinks corresponds to large $k_\times$ and soft crosslinks corresponds to small $k_\times$. The force is measured with respect to the Euler buckling force $f_b = \frac{\pi^2\kappa_f}{2L^2}$.

3 Results

3.1 Unbinding of crosslinks under force

In this sub-section we consider the effects of unbinding under increasing levels of force. To this end, we set $k_\times \to nk_\times$ in Eq. (1) and determine the equilibrium state by minimization with respect to $\theta(s)$ and n. Defect formation will not be allowed in this section, thus we take $d(s) \equiv 0$.

The minimization with respect to the variable $\theta(s)$ gives a differential equation, namely,

$$\theta''(s) - nK^2\theta(s) = -\frac{f}{\kappa_f} \qquad K^2 = \frac{k_\times b^2}{2\kappa_f\delta}, \qquad (6)$$

solving which we get the behaviour of $\theta(s)$. The bending angle satisfies the proper boundary conditions that $\theta(0) = 0$, $\theta'(L) = 0$ and that $\theta(s)$, $\theta'(s)$ are continuous everywhere. The bending angle is $\theta(s) \propto f$, more explicitly,

$$\theta(s) = \frac{f}{K^2\kappa_f}\left[1 - \frac{\cosh K(L-s)}{\cosh KL}\right]. \qquad (7)$$

Therefore, the effective free energy per crosslink site including entropy of mixing is,

$$F(n) = \frac{f^2 \operatorname{sech}^2(\sqrt{n}KL)}{8n^{3/2}K^3\kappa_f} \left[(10 - 3n)\sinh(2\sqrt{n}KL) \right.$$
$$-2\sqrt{n}KL(6 - 2n + (4 - n)\cosh(2\sqrt{n}KL)) \right]$$
$$+ \mu\,n + k_B T[n\log n + (1 - n)\log(1 - n)]. \quad (8)$$

At zero temperature, the free energy has minimum either at $n = 0$ or $n = 1$. The crosslink density corresponding to the lowest energy jumps from 1 to 0 as we reach a critical value of force f_c. This means that at f_c, suddenly all crosslinks unbind and the bundle breaks down into two independent filaments. The phase diagram can be found by equating $F(0) = F(1)$ (see Fig.4).
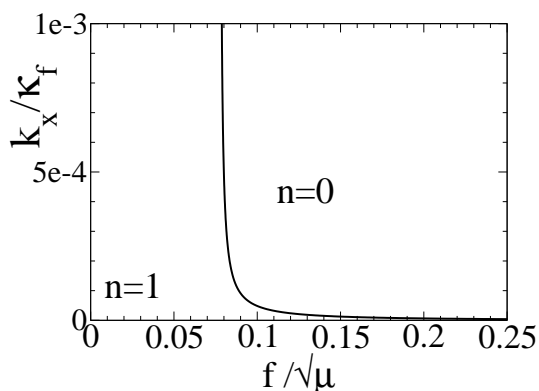
Fig. 4. Phase diagram for inextensible filaments at temperature $T = 0$. The transition across the line separating the phases with average crosslink density $n = 0$ (fully decoupled) and $n = 1$ (fully coupled) is discontinuous.

At finite temperatures, there is a variation in the crosslink density n with the driving force f (see Fig. 5). The crosslinks unbind continuously with increasing force for soft crosslinks (small $k_\times$) while for large $k_\times$, there is a jump in the crosslink density indicating a first-order transition. The transition is from a state where the filaments are tightly coupled by many bound cross-links, to a state of nearly independent filaments with only a few bound crosslinks. This happens due to the presence of a metastable state at large $k_\times$. The plot of the crosslink density with force, therefore, shows a region where for a given force two values of n are possible. The exact location of the jump in the crosslink density from one branch to the other can be determined by observing when the global minimum and the metastable minimum switch. This is the case for slow quasi-static driving, when crosslinks are allowed to equilibrate for a given level of the external load. Away from equilibrium, the forward and the reverse branch will be different depending on the driving frequency, giving rise to interesting dynamics and hysteresis effects. This will be discussed later in Sect.4. The range of f, when there is a metastable state, increases with increasing crosslink stiffness. For very large crosslink stiffness, the allowed values of n are more towards the two extremes, 1 and 0, like
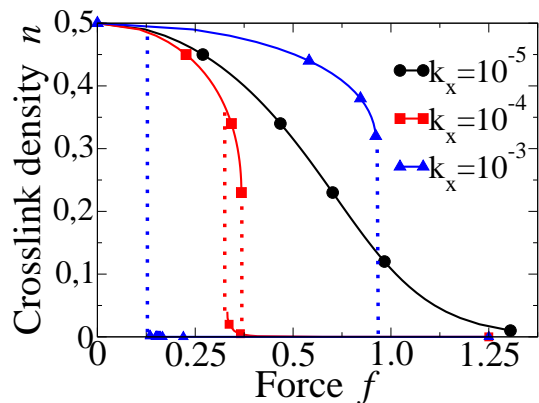
Fig. 5. The variation of the crosslink density with driving force at finite temperature and $\mu = 0$. In this figure, for $k_\times = 10^{-4}$ and $k_\times = 10^{-3}$, the jump from one to the other branch happens within the region enclosed by the dotted line.

zero temperature behaviour. For a bundle consisting of more than two filaments, a series of first-order transitions is expected as observed in Ref. [25].

The discontinuity in the crosslink density with force is reflected in the average bending angle

$$\langle\theta\rangle = \frac{1}{L}\int_0^L \theta(s)ds, \quad (9)$$

which is feasible to observe in experiments. In Fig.6, we plot $\langle\theta\rangle$ as a function of force f. We see that the slope of the curve $\langle\theta\rangle$ gradually reaches to a fixed value for all $k_\times$, which corresponds to the value with $n = 0$. For large $k_\times$, the average bending changes suddenly from small value to a large one as a result of jump in the crosslink density. The softer the crosslinks, the smaller is the jump in the average bending at the critical fo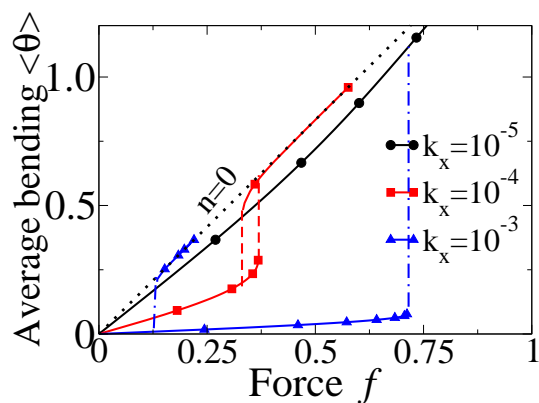rce. For the last two graphs, we set the chemical potential $\mu = 0$. Nonzero μ tends to lead to stronger discontinuities.

Fig. 6. This plot shows how the average bending $\langle\theta\rangle$ of the bundle varies with the driving force f ($\mu = 0$). The black dotted line shows the behaviour for $n = 0$. All the lines merge gradually to this dotted line for large force.

This sudden unbinding of nearly all crosslinks is reminiscent of a brittle failure process during which bundle integrity is lost completely. With our choice of boundary conditions (grafted at one end), filaments stay together, however, and after removal of the load, crosslinks can again form. This will be a quick process which is essentially downwards in energy landscape. This is illustrated by Fig. 7.

A system with similar kind of unbinding mechanism is a double stranded DNA. Force-induced phase transitions by pulling two strands in opposite direction is discontinuous from a fully bound or zipped state to a fully unbound or unzipped state [31]. This all-or-none binding state resembles the case of the f-actin bundle with very stiff crosslinks.
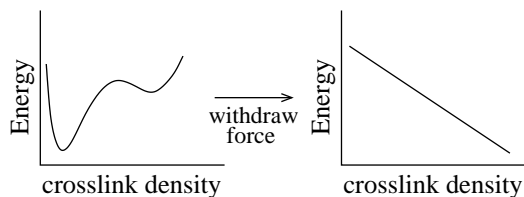

Fig. 7. Schematic of the energy landscape with and without force. At large forces, the bundle is in an unbound state with the minimum of the energy at very small n. At this condition, keeping all other parameters fixed, if we withdraw the force, the energy profile is linearly decreasing with n, with the minimum at $n = 1$. Hence, after only a short time we see the system to roll back to the bound state, regaining its old configuration with perfectly ordered bound crosslinks as it was before the deformation.

3.2 Rebinding of crosslinks under force

In this section we consider the possibility that, under deformation, crosslinks rebind to more favourable binding sites, thus forming a defect. As explained in the modelling section this is accounted for by a defect-function $d(s)$, which goes from zero to δ at the defect site s_D. The relevant observable now becomes the defect site s_D instead of the crosslink density n, which we assume to be saturated at $n = 1$. The differential equation for $\theta(s)$, obtained by minimizing the Hamiltonian w.r.t. θ, is

$$-2\kappa_f \theta''(s) + \frac{k_\times b}{\delta}(b\theta(s) - d(s)) = 2f. \qquad (10)$$

One can find the total energy E as a function of defect site s_D using the solution $\theta(s)$ of this differential equation in the Hamiltonian. The value of s_D at which E is lowest in the E vs. s_D curve gives the location of the defect. Without force, $f = 0$, it is at the free end, $s_D = L$. As the force increases, beyond a critical force, the bundle creates a defect to reduce bending stress and crosslink shearing. There is a region near the free end of the bundle where the creation of a defect is very costly. This region widens with increasing crosslink stiffness and vanishes for

soft crosslinks. Hence, for large $k_\times$, when increasing force from a very small value, we see a sudden creation of defect deep inside the bundle at the critical force. Fig. 8 shows the location of the defect scaled by the length of the bundle L, vs. force f. The critical force f_c is the value of force where the defect site jumps from $s_D = L$ to smaller value. As the force increases further, the defect site moves towards the fixed end and gets stuck there.
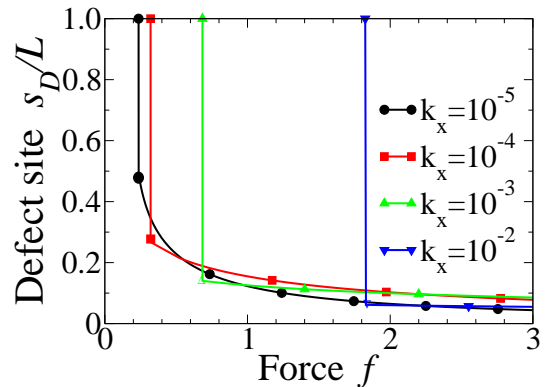

Fig. 8. Defect site s_D moves with the driving force f. The critical force f_c is the value of force where the lines jump to $s_D = L$.

The creation of the defect is also apparent in the value of the average bending angle $\langle\theta\rangle$, which displays a sudden jump. We plot $\langle\theta\rangle$ against force for different values of $k_\times$ in Fig. 9. For soft crosslinks the average bending angle increases stronger with increasing force than that of stiff crosslinks. Rather, for very stiff crosslinks, the average bending does not change much with increasing force except at the critical force, where we see a jump in the value of $\langle\theta\rangle$. In this limit the bundle is extremely stiff and can hardly be bent by the external force – any bending deformation would lead to very costly shearing of the crosslinks, which is avoided as long as no defect forms. With a defect present, the bend is localized to the defect region leaving most of the bundle straight and thus the crosslinks unstrained.

This results in a kink in the bundle. Fig.10 shows how the bundle looks like for soft ($k_\times = 10^{-3}$) and stiff crosslinks ($k_\times = 10^{-1}$) for a large force, $f = 5f_b$. For comparison, we fix the defect position at $s = L/2$ in both the bundles. We see that for large $k_\times$, there is a sharp bending, or kink, around the defect site. The larger $k_\times$, the sharper is the kink. For small $k_\times$ no kink is visible, even with a defect. The light blue line in Fig. 10 shows the bundle for extensible filament with the same crosslink stiffness ($k_\times = 10^{-1}$) as the kinked bundle (black line) with inextensible filaments. From this graph we can conclude that the kink can be suppressed either by allowing stretching in the filaments or by choosing soft crosslinks.

The stretching of the filaments will modify the shearing Hamiltonian by an extra contribution of relative displacement $u(s)$ of the crosslink binding sites of one filament with respect to the other in the integrand, $b\theta(s) \rightarrow$
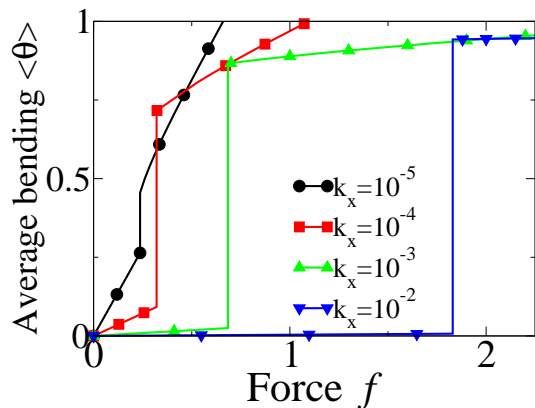
Fig. 9. The average bending $\langle\theta\rangle$ as a function of driving force f for various crosslink stiffness $k_\times$.
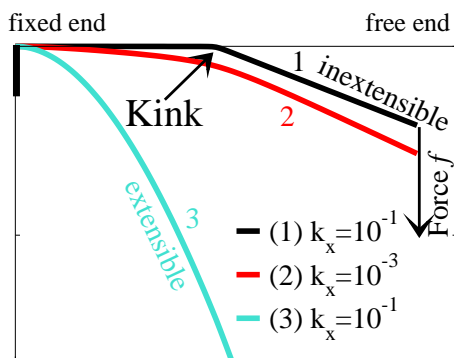

Fig. 10. Bundle contours for different crosslink stiffness. All the bundles have a defect at $s_D = L/2$. The sharpness of bending is much higher in the bundle with stiff crosslinks. The light coloured steep line (3) shows the bundle with extensible filaments.

$u + b\theta(s)$. Also there will be an extra term in the Hamiltonian coming from the stretching energy of the Hamiltonian, *viz.*,

$$H_{st} = \frac{k_s \delta}{2} \int_0^L u'^2(s)\, ds. \tag{11}$$

The phase diagram in Fig. 11 shows that the critical force f_c increases with increasing $k_\times$. For very small value of $k_\times$, f_c saturates to a fixed finite value, indicating that no matter how soft the crosslinks are, there will be a possibility to create a defect in the bundle by applying force. In this graph, additionally, we indicate the phase separation line for bundles with extensible filaments (dashed line). If we allow stretching of the filaments, an additional deformation mode becomes available that the bundle can use to minimize energy. Thus, stretching delays the creation of a defect. So, for same crosslink stiffness, it is easier to create a defect in bundles with inextensible filaments.

Now let us consider a bundle which has been exposed to a large force and held in the deformed configuration for a long time, so that there is creation of a defect deep inside the bundle. In this configuration, the energy $E(s_D)$ has a minimum at small s_D with a large energy barrier towards higher values of s_D (see Fig. 12). If, at this point,
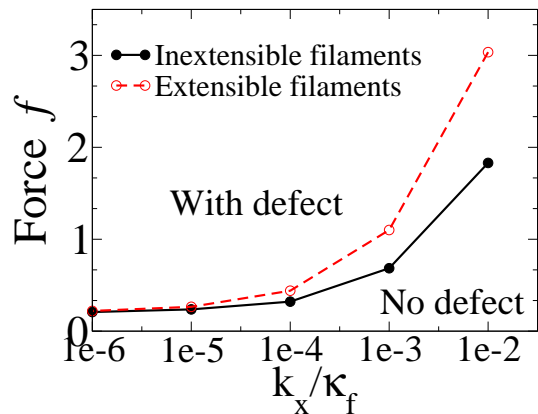

Fig. 11. The phase diagram of a bundle with inextensible filaments at zero temperature. The line separates the phases with a defect and with no defect. For small $k_\times$, the critical force becomes independent of $k_\times$. The dashed line shows the behaviour for extensible crosslinks.

we remove the force, then $E(s_D)$ has a wide plateau except at the two ends, the lowest energy now being for a defect at the free end (i.e. no defect). Once the defect is created in the bundle, and if the force is withdrawn, the defect gets trapped in the plateau as it does not feel any driving force to move towards the free end, where it can escape (see Sect. 4.2). Within this time scale, even without any driving force, we see the bundle in a plastically deformed configuration. This mechanism, which is reminiscent of the ductile failure of metals, may very-well be responsible for the long-lived residual deformation that has been observed in the experiments of Strehle *et al.* [23].
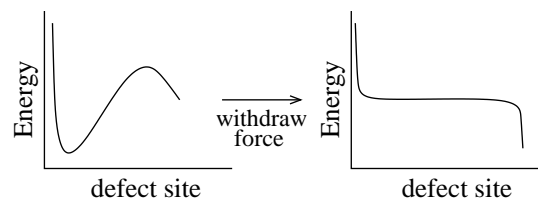

Fig. 12. Schematic of the energy landscape with and without force. At large forces, the bundle is in a kinked state with a defect present at small s_D. If we withdraw the force, the energy is flat and independent of s_D. This means that there is only a weak driving force for the defect to move towards the free end, where it can escape. Thus, depending on the dynamics of the defect, the bundle remains in its plastically deformed state for a long time.

4 Dynamics

Let us now consider some aspects of the dynamical evolution of the bundle degrees of freedom. In general, this will represent a coupled evolution of the bundle contour, represented by $\theta(s)$, and the binding state of the crosslinks, for example given in terms of the average occupation n

or the defect location s_D. In what follows we will present simplified approaches to deal with two scenarios of time-dependent forcing: oscillating force, and switch-off after constant force.

4.1 Crosslink dynamics

Here, we consider the brittle failure scenario of Section 3.1 and ask about the dynamical evolution of the crosslink occupation $m = n \cdot N_\times = 0, 1, \ldots, N_\times$.

If bundle conformational degrees of freedom (bending mode θ and possibly internal stretching modes) are assumed to be relaxed one can formulate a one-step Master equation for the temporal evolution of the probability distribution $p_m(t)$

$$\frac{\partial p_m}{\partial t} = r_{m+1}p_{m+1} + g_{m-1}p_{m-1} - (r_m + g_m)p_m, \quad (12)$$

with the rates

$$r_m = m e^{\beta \Delta E_m(f)} r_0, \qquad g_n = (N_\times - m) r_0.$$

r_0 represents an intrinsic rate constant and the free energy profile $\Delta E_m(f)$ should be taken from Section 3.1. A similar problem is the cluster of adhesion sites discussed in Ref. [32]. There, the energy profile is taken to be linear in the applied force, which is divided among all bound sites, $r_m = m e^{f/m} r_0$. Here, the dependence on force is, in general, more complex. It is also illustrative to consider the general case in the framework of the associated rate-equation

$$\dot{m} = -m r_0 e^{\beta \Delta E_m} + r_0(N_\times - m), \quad (13)$$

When ΔE_m depends on m, this equation follows from the Master equation Eq. (12) only by making the approximation $\langle r_m \rangle \rightarrow r_{\langle m \rangle}$. As expected from the results of Section 3.1 (see Fig. 5) this equation either has one stable stationary state (at low or high force), or two stable states (at intermediate force).

The full stochastic trajectory of the bundle occupation $m(t)$ in response to time-dependent forces can only be obtained by solving the Master equation Eq. (12). For oscillating forces $f(t) = f_0 \sin(\omega t)$, for example, one expects to see ω-dependent hysteresis effects, due to the presence of an energy barrier between the metastable state and the groundstate. The size of the energy barrier depends on force, $\Delta E(f)$, as calculated in Section 3.1. With this dependence we can set up a simplified treatment of barrier crossing events that lead to hysteresis without having to solve the full Master equation. To this end, we use Kramers equation for the rate r of a thermally assisted escape over an energy barrier

$$\Delta E(f) = -k_B T \ln \frac{r}{\hat{r}_0}, \quad (14)$$

where $\hat{r}_0$ corresponds to some intrinsic attempt rate. By mapping escape rate to frequency, $r/\hat{r}_0 \equiv \omega/\omega_0$, we can

establish a relation $f(\omega)$, for the force at which the barrier can be crossed. Fig. 13 shows examples of the resulting hysteresis loops for two different frequencies. As expected, the area within the hysteresis loop is reduced when the frequency decreases. The frequency range over which hysteresis can be observed depends on the size of the energy barriers. For small values of the chemical potential μ, the barriers may only be a few $k_B T$. In this limit our approach is not expected to hold.
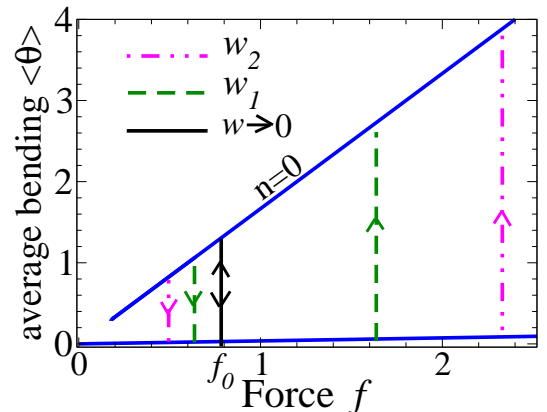

Fig. 13. Hysteresis loops for the average bending angle $\langle \theta \rangle$ vs. force f for different frequencies ($\mu = 0.01$). The black line corresponds to the small frequency limit, i.e. to the equilibrium transition. The green dashed line is for frequency $w/w_0 = 0.135$ (w_1) and the magenta dashed-dotted line corresponds to the frequency $w/w_0 = 0.368$ (w_2) . Larger frequency indicates larger hysteresis loop.

4.2 Coupled dynamical evolution of crosslinks and filament conformation

Here, we discuss the ductile failure mechanism introduced in Section 3.2. In particular, we are interested in the relaxation of the bundle contour after the force is switched off. This situation is analogous to the experimental set-up of Ref. [23]. The relaxation represents a coupled dynamical evolution of the bundle contour $y(s,t)$ (with $y' \equiv \theta$) and the defect location $s_D(t)$. For the contour one can derive the equation of motion from the Hamiltonian Eqs. (2) and (4).

$$\zeta \frac{\partial y}{\partial t} = -2\kappa_f y^{(4)} + \frac{k_\times b}{\delta}(by'' - d') \quad (15)$$

which represents the time-dependent generalization of Eq. (10) for $f = 0$.

For the temporal evolution of the defect position s_D we use a simple rate equation

$$\frac{\partial s_D}{\partial t} = r\delta \tanh(\beta \Delta E/2) \quad (16)$$

where the distance between crosslink binding sites δ represents the length-scale for the defect motion; the rate r

sets the relevant time-scale. It will depend, for example, on the chemical potential of the crosslinks, $r \sim e^{\beta\mu}$.

The tanh-factor derives from the activated nature of the process. For the defect to move the distance δ, two energy barriers need to be crossed: first a crosslink has to unbind from its old binding site. Second, it needs to "stretch-out" to reach its new binding site. These two processes are illustrated in Fig. 14.
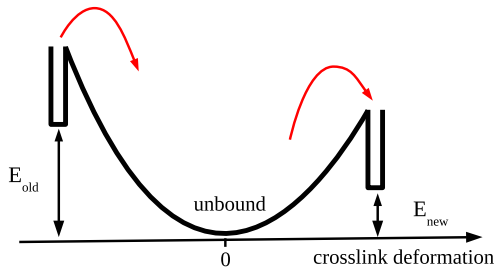

Fig. 14. Illustration of the energy landscape relevant for the motion of a defect. The defect moves by δ, when one crosslink, first, unbinds and then rebinds to a neighboring site. The relative energy gain is $\Delta E = E_{\text{old}} - E_{\text{new}}$.

The two Equations (15) and (16) have to be solved in parallel, with the defect location entering the function d in Eq. (15), and the bundle contour determining the energy gain ΔE in Eq. (16). This is achieved via a mode-decomposition of the bundle contour

$$y(s,t) = y_{\text{part}} + \sum_q \psi_q(s)\tilde{y}_q(t) \qquad (17)$$

where the ψ_q are the Eigenfunctions of the operator $-\partial_s^4 + \kappa_\times\partial_s^2$ [1], and we separate out a particular solution y_{part} of the equation. The resulting equations are integrated numerically with a simple explicit Euler step.

Fig. 15 displays the results of such a calculation. Depicted is the average bending angle $\langle\theta\rangle$ as a function of time and for various values of the time-scale r^{-1} for defect motion. The bundle is initialized in a highly bent state with a defect at position $s_D = 0.1$.

Before complete relaxation into its final straight state ($\langle\theta\rangle = 0$), the bundle passes through different stages. On small time-scales the evolution is independent of r^{-1} and signals the relaxation of the bundle contour for an immobile defect. Once this fast process is completed the final relaxation is slaved to the motion of the defect. This is illustrated by the data collapse when plotted vs. rt as demonstrated in the inset. In the plateau region the defect does not move as the driving force for motion is very small (ΔE is small, see Fig. 12). Depending on the time-scale for defect motion and also on the crosslink stiffness $k_\times$, the bundle may remain in this plastically deformed state for a long time. Finally, the defect starts to move, leading

---

[1] The functions are given by $\psi_q = A\sin(qx) + B\cos(qx) + C\sinh(\tilde{q}x) + D\cosh(\tilde{q}x)$, where $\tilde{q}^2 = q^2 + \kappa_\times$ and the constants as well as the wavenumbers q are determined from the boundary conditions.
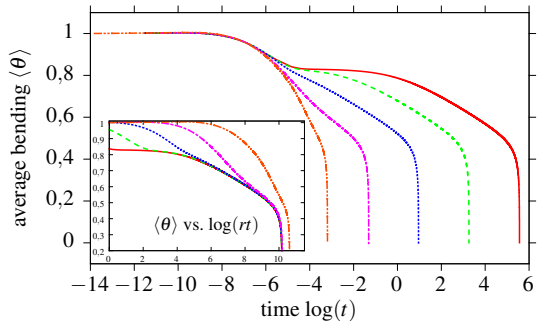

Fig. 15. Average bending angle $\langle\theta\rangle$ vs time t for different values of the time-scale $r^{-1} = 10^{-6} \ldots 10^{-2}$ (from left to right) and for $k_\times = 10^{-2}$.

to a logarithmically slow terminal relaxation, after which the defect leaves the bundle.

5 Summary and Outlook

In this paper, we study the response of F-actin bundles to driving forces through a simple analytical model. We consider two filaments connected by reversibly bound crosslinks and driven by a force applied at the ends. Our model relies on the fact that under large deformation, the crosslinks un- and re-bind in order to reduce the stress in the bundle.

We can define two failure modes under load. *Brittle failure* is observed when crosslinks suddenly unbind, leading to catastrophic loss of bundle integrity. *Ductile failure* maintains bundle integrity at the cost of crosslink remodelling and defect formation.

We present phase diagrams for the onset of failure, highlighting the importance of crosslink stiffness for these processes. Crossing the phase boundaries, force-deflection curves display (frequency-dependent) hysteresis loops, reflecting the first-order character of the failure processes.

We also relate our findings to recent experiments that evidence long-lived plastically-deformed actin bundles [23]. To this end we combine an elasto-hydrodynamic description of the bundle relaxation with a rate equation for defect motion. The terminal relaxation of the plastic deformation is thus seen to be slaved to the dynamics of the defect. For weak crosslinks a defect is spread over the entire length of the bundle and is not discernible in the bundle contour. For stiff crosslinks defects take the form of well localized kinks. These kinks only have a very small tendency to move towards the free end of the bundle, where they can escape. Thus, crosslink stiffness is a key factor governing the long-time dynamics of the bundle.

The model should be extended towards a more realistic bundle architecture, with more than just two filaments and in three spatial dimensions. Similarly, it would be useful to consider more than one defect and also different types of defects. Finally, it would be interesting to analyze in more detail the transition between brittle and ductile behavior, when, for example, the binding enthalpy of the linkers is varied. These questions will have to be

tackled with the help of suitable simulation techniques and are left for future work.

References

1. A. E. Cohen and L. Mahadevan, Proc. Natl. Acad. Sci. U.S.A. **100**, (2003) 12141-12146.
2. A. Ceber, Z. Dogic, and P. A. Janmey, Phys. Rev. L **96**, (2006) 247801.
3. DeRosier, D., Tilney, L. and Flicker, P. , J. Mol. Biol. **137**, (1980) 375.
4. Fygenson, D. K., Marko, J. F. and Libchaber, A., Phys. Rev. Lett. **79**, (1996) 44974500.
5. A. Mogilner and B. Rubinstein, Biophys. J. **89**, (2005) 782.
6. E. Atilgan, D. Wirtz, and S. X. Sun, Biophys. J. **90**, (2006) 65.
7. D. Vignjevic, S. Kojima, Y. Aratyn, O. Danciu, T. Svitkina, and G. G. Borisy, J. Cell Biol. **174**, (2006) 863.
8. A. J. Hudspeth and D. P. Corey, Proc. Natl. Acad. Sci. U.S.A. **74**, (1977) 2407.
9. M.M.A.E.Claessens,M.Bathe,E.Frey,andA.R.Bausch, Nat. Mater. **5**, (2006) 748.
10. J. H. Shin, L. Mahadevan, P. T. So, and P. Matsudaira , J. Mol. Biol. **337**, (2004) 255.
11. J. H. Shin, M. Gardel, L. Mahadevan, P. Matsudaira, and D. A. Weitz , Proc. Natl. Acad. Sci. U.S.A. **101**, (2004) 9636.
12. M. M. A. E. Claessens, C. Semmrich, L. Ramos, and A. R. Bausch, Proc. Natl. Acad. Sci. U.S.A. **105**, (2008) 8819.
13. K. R. Purdy, J. R. Bartles, and G. C. L. Wong, Phys. Rev. Lett. **98** , (2007) 058105.
14. H. Shin, K. R. Purdy Drew, J. R. Bartles, G. C. L. Wong, and G. M. Grason , Phys. Rev. Lett. **103**, (2009) 238102.
15. L. Haviv, N. Gov, Y. Ideses, and A. Bernheim-Groswasser, Eur. Biophy. J. **37**, (2008) 447.
16. M. Bathe et al., Biophys. J. **94**, (2008) 2955.
17. C. Heussinger, M. Bathe, E. Frey, Phys. Rev. Lett. **99**, (2007) 048101 , http://link.aps.org/doi/10.1103/PhysRevLett.99.048101
18. P. Benetatos and E. Frey, Phys. Rev. E **67** , (2003) 051108.
19. J. Kierfeld, T. Kühne, and R. Lipowsky, Phys. Rev. Lett. **95** , (2005) 038102.
20. J. Kierfeld, Phys. Rev. Lett. **97**, (2006) 058302.
21. G.M. Grason, Phys. Rev. E **79**, (2009) 041919.
22. C. Heussinger, G.M. Grason, J. Chem. Phys. **135**, (2011) 035104.
23. D. Strehle, J. Schnauss, C. Heussinger, J. Alvarado, M. Bathe, J. Ks, and B. Gentry, Eur. Biophys. J. **40**, (2011) 93.
24. C. Heussinger, Phys. Rev. E **83**, (2011) 050902(R).
25. R. L. C. Vink and C. Heussinger, JCP **136**, (2012) 035102.
26. R. Everaers, R. Bundschuh, K. Kremer, Europhys. Lett. **29**, (1995) 263.
27. S. Camalet, F. Jülicher, J. Prost, Phys. Rev. Lett. **82**, (1999) 1590.
28. A. Hilfinger, F. Jülicher, Phys. Biol. **5**, (2008) 016003.
29. C. Heussinger, F. Schüller, E. Frey, Phys. Rev. E **81**, (2010) 021904 , http://link.aps.org/doi/10.1103/PhysRevE.81.021904
30. J. Käs, H. Strey and E. Sackmann , Nature **368**, (1994) 226 - 229.
31. S. M. Bhattacharjee, J. Phys. A 33 **33**, (2000) L423, cond-mat/9912297.
32. T. Erdmann, U. S. Schwarz, Phys. Rev. Lett. **92**, (2004) 108102, http://link.aps.org/doi/10.1103/PhysRevLett.92.108102